 MCB, vol.10, no.1, pp.27-42, 2013

Derivation of the Stress-Strain Behavior of the constituents of Bio-Inspired Layered TiO_2/PE-Nanocomposites by Inverse Modeling Based on FE-Simulations of Nanoindentation Test

G. Lasko*, I. Schäfer*, Z. Burghard†, J. Bill†, S. Schmauder*
U. Weber* and D. Galler‡

Abstract: Owing to the apparent simple morphology and peculiar properties, nacre, an iridescent layer, coating of the inner part of mollusk shells, has attracted considerable attention of biologists, material scientists and engineers. The basic structural motif in nacre is the assembly of oriented plate-like aragonite crystals with a 'brick' ($CaCO_3$ crystals) and 'mortar' (macromolecular components like proteins) organization. Many scientific researchers recognize that such structures are associated with the excellent mechanical properties of nacre and biomimetic strategies have been proposed to produce new layered nanocomposites. During the past years, increasing efforts have been devoted towards exploiting nacre's structural design principle in the synthesis of novel nanocomposites. However, the direct transfer of nacre's architecture to an artificial inorganic material has not been achieved yet. In the present contribution we report on laminated architecture, composed of the inorganic oxide (TiO_2) and organic polyelectrolyte (PE) layers which fulfill this task.
To get a better insight and understanding concerning the mechanical behaviour of bio-inspired layered materials consisting of oxide ceramics and organic layers, the elastic-plastic properties of titanium dioxide and organic polyelectrolyte phase are determined via FE-modelling of the nanoindentation process. With the use of inverse modeling and based on numerical models which are applied on the microscopic scale, the material properties of the constituents are derived.

Keywords: Nanoindentation, stress-strain constitutive law, inverse modeling, bio-

* Institute for Materials Testing, Materials Science and Strength of Materials, University of Stuttgart, Pfaffenwaldring 32, D 70569, Stuttgart, Germany. E-mail: galina.lasko@imwf.uni-stuttgart.de
† Institute of Materials Science, University of Stuttgart,Heisenbergstrasse 3, D 70569 Stuttgart, Germany.
‡ Stuttgart University, 070569, Stuttgart, Germany.

mimetics

1 Introduction

Biomaterials are perfect models for specialized materials that can reveal amazing combinations of mechanical properties. Some of their properties such as stiffness, hardness and fracture toughness are hardly attained by artificial materials (1). Nacre, which is the inner layer of mollusk shells, shows a high performance. Also it is build out of relatively weak components. Based on this prototype, new materials can be developed which are stiff but also have high fracture toughness. One example of the bio-inspired synthesis route to inorganic layers is the chemical bath deposition technique (CBM) (2). Combined with the layer-by-layer technique it was possible to create Titandioxide (TiO_2)/ Polyelectrolyte (PE) multilayered films with a nacre-like architecture (3). The chemical bath deposition method operates at low temperatures (30–100°C), similar to the biomineralization process that occurs in natural organic–inorganic nanocomposites. One of the main problems is that the constitutive properties of the components of the nanocomposites are almost unknown. For macroscopic objects there exists the possibility of verification of the constitutive behavior of the constituents by comparison of the stress-strain curves obtained by inverse modeling with the experimentally obtained ones. When performing an analysis of the thin coatings, the performance of experimental tests is difficult or even impossible and here a simple and easy method to define the mechanical properties is the nanoindentation technique. Nanoindentation testing was carried out with a scanning nanoindenter including a depth-sensing force transducer (HysitronTriboScope), combined with a commercial scanning probe microscope (NanoScope III Multimode, Digital Instruments). Indentations were made with a cube corner diamond indenter with a nominal tip radius of $\sim$40 nm. In all experiments, a maximum force of 80 μN was applied, which yields a penetration depth of about 100 nm. In the present work, we report on the computer simulation of mechanical properties of the components of this nanocomposite film, composed of alternating layers of TiO_2 as inorganic component and PE as the organic component. The stress-strain behavior of separate phases of the nanostructured layered TiO_2/PE nanocomposite are analyzed, and have been inversely obtained by numerical modeling with the finite element (FE) method of nanoindentation test of separate phases of the TiO_2/PE nanocomposite. For the first time, the stress-strain curves of the constituents of the bio-inspired TiO_2/PE layered nanocomposite have been determined by coupling the results of the experiments with the FE simulations of nanoindentation.

2 Definition of Young's modulus from nanoindentation tests

Based on the indentation load-displacement data, mechanical properties such as hardness and Young's modulus of the solid-supported film can be determined. In experiments (2, 3) a cube corner indenter has been used instead of the usually used Berkovich indenter. Moreover, the cube corner indenter is sufficiently sharp (tip radius ∼40 nm) to allow scanning of the surface in order to identify positions that are flat enough for indentation (Figure 1a). In addition, it enables creating plastic deformation within small indentation depths, which ensures remaining within the plastic and elastic field of the film, and minimizing the impact of the substrate which is crucial for investigating very thin films. In all experiments, initially a standard calibration of the tip was carried out on fused quartz within the penetration depth range of 3 to 100 nm. This procedure yielded for the hardness H = 9.3 GPa ± 0.3 and the Young's modulus E = 69.5 ± 1.67 GPa. In general, nanoindentation data obtained at shallow penetration depths are affected by the surface roughness of the sample, and the substrate has a noticeable influence for indentation depths larger than 20 % of the total film thickness (4). Thus, in order to take these limitations into account, the nanoindentation data were evaluated in the contact depth range between 10 % and 20 % of the total film thickness. The obtained data were evaluated using the method described by Oliver and Pharr (4).

The indentation force was varied during subsequent load/partial unload-cycles over 25 steps, with automatic recording of the indentation depth after each step. For each specimen, the results were averaged over fifteen indentations made at different locations.

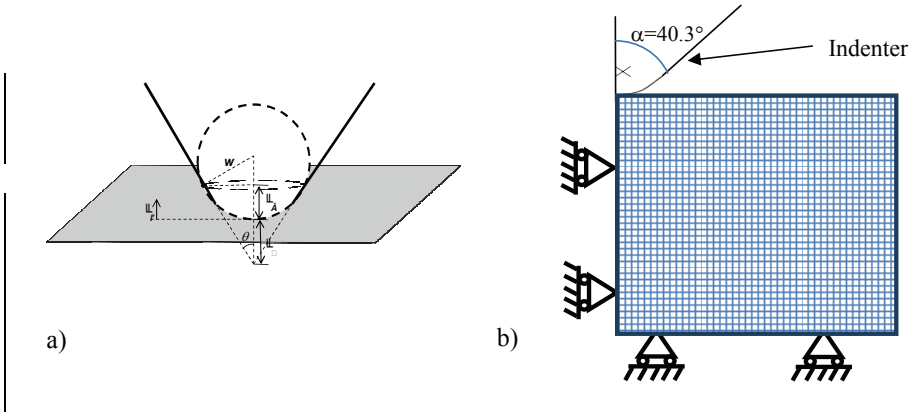

Figure 1: a) The sketch of the tip radius geometry of the used intender in the FE-simulation; b) model with boundary conditions.

According to Oliver and Pharr (4), the hardness H of the tested material is given as the maximal applied load P_{max} (read from the load-displacement curve) divided by the projected contact area of the indentation at this load A_c:

$$H = \frac{P_{\max}}{A_c} \tag{1}$$

The contact area A_c is considered as an area function of the contact depth h_c:

$$A_c = F(h_c) = C_0 h_c^2 + C_1 h_c + C_2 h_c^{1/2} + C_3 h_c^{1/4} + C_4 h_c^{1/8} + C_5 h_c^{1/16} \tag{2}$$

where C is 2.598 for a cube corner probe, $C_i (i$ = 1-5) are positive coefficients, F is the force and the contact depth h_c is given by the equation:

$$h_c = h_{\max} - \varepsilon \cdot \frac{P_{\max}}{S} \tag{3}$$

The latter term describes the deflection of the surface at the contact parameter. The geometric constant ε is founded on the geometry of the indenter tip (ε = 0.75) and the initial unloading contact stiffness S. S is the slope of the upper portion of the unloading curve during the initial stage of unloading and is defined as following equation:

$$S = \frac{dP}{dh} \tag{4}$$

The reduced elastic modulus E_r can be calculated from the contact area A_c and the unloading contact stiffness S as follows:

$$E_r = \frac{\sqrt{\pi}}{2\sqrt{A_c}} \cdot S \tag{5}$$

The reduced elastic modulus E_r is defined by the Young's modulus of the sample E_s:

$$\frac{1}{E_r} = \frac{\left(1 - \upsilon_i^2\right)}{E_i} + \frac{\left(1 - \upsilon_s^2\right)}{E_s} \tag{6}$$

The symbols ν and E denote the Poisson's ratio and Young's modulus for the sample with subscript s and the indenter material with subscript i. In the experiments, the nanoindenterconsists out of diamond with E_i = 1141 GPa and ν_I = 0.07.

According to the procedure described above the Young's modulus of pure titanium dioxide and polyelectrolyte have been obtained from nanoindentation. The averaged Young's modulus of over 50 indents in cross sections as well as the surface for the different indentation depth have been obtained and are equal to 27 GPa for TiO_2 and 5 GPa for PE.

3 Finite element modeling of nanoindentation

Limited studies are available to obtain the plastic properties with the nanoindentation technique. Therefore, the indentation loading process is simulated with the Finite Element Method (FEM) and the software ABAQUS/CAE (Version 6.11-1, Dassault Systemes Simulia Corp., Providence, RI, USA), assuming finite deformation characteristics. Instrumented indentation using a conical indenter (shown in Fig. 1a) has been simulated assuming axisymmetric and frictionless contact. For the simulation of deformation response of the pure titanium dioxide layer and the pure PE layer 80000 four-node axisymmetric elements (CAX4) were used.

The model of the indenter used in the present simulations has a conical shape with a tip-radius of 40 nm and a semi vertical angle of 40.3° which gives the same area to depth function as that of a cube-corner indenter, used in the experiment. Since large deformation takes place near the indenter tip, mesh refinement was accomplished near the contact zone. The conical indenter was modeled by the use of an analytical rigid surface. Symmetry boundary conditions were applied to the cut faces of the quadrant while the remaining edges were unconstrained in the modeling of indentation by a conical indenter. In the case of indentation of the conical indenter the nodes along the axis of rotation were free to move only along the Y-axis (Fig. 1b).

By applying a downward displacement to the rigid body reference node of the indenter the indentation process was simulated. The indentation depth was measured from the displacement of the node, situated directly under the indenter tip, i. e. at the point of first contact and the indentation load for the conical indenter was the reaction force of the reference node of the rigid indenter.

The friction between the material and indenter does not require special consideration and can be omitted in the inverse analysis (5).

For the definition of the plastic properties of the constituent phases (TiO_2 and PE) the method of inverse modeling has been applied in two steps:

At first, the stress-strain curve for pure titanium dioxide has been obtained by comparing the P-h curve obtained from the FE-calculations with the experimentally obtained one for pure titanium dioxide. The second step was to follow the same procedure for the stress-strain curve of polyelectrolyte.

Shown in Fig. 2 is the force-penetration curve that has been obtained in the experiment. Nanoindentation tests have been performed till the penetration depth being equal to 120 nm following the procedure loading-unloading, the maximum force attained in the experiment was around 80 μN and the penetration depth around 120 nm. The material is supposed to be homogeneous, isotropic and elasto-plastic using the classical plasticity model with von Mises criterion.

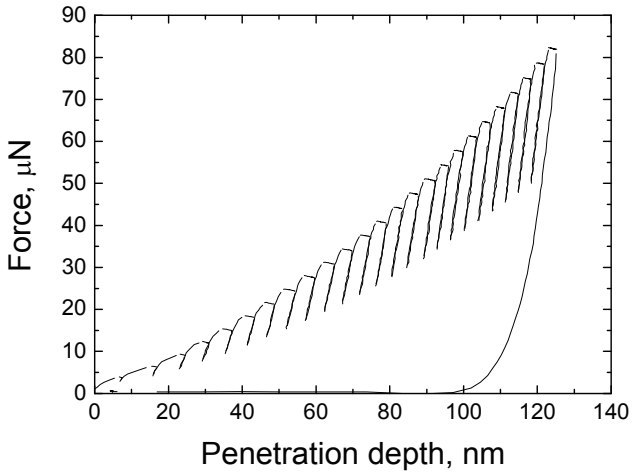

Figure 2: The experimentally obtained force-penetration depth-curve for TiO_2 from nano indentation.

4 Basic constitutive laws used for definition of stress-strain behavior of material via inverse modeling

There exist several models used in inverse modeling of the constitutive behavior: Hollomon's model (6), Ramberg-Osgood (7) and bilinear material models (8).

The Hollomon's model defines the power law relationship between the stress of the material and the value of plastic strain:

$$\sigma = \sigma_y + K\varepsilon_p^n \tag{7}$$

where σ_y is the flow stress, K is the hardening coefficient, ε_p is the plastic strain and n is the strain hardening exponent.

The advantage of using the simple Hollomon relationship (6) is the necessity of determining two unknown parameters, what is essential for keeping the costs of computational testing of the proposed inverse methods low.

The Ramsberg-Osgood model (7): it describes the non-linear relationship between strain and stress, which is normally defined by a stress-strain curve resulting from an experiment. The following equation defines the strain:

$$\varepsilon = \frac{\sigma}{E} + \alpha \left(\frac{\sigma}{\sigma_0}\right)^{n-1} \frac{\sigma}{E} \tag{8}$$

where ε is the strain, σ_0 is the yield stress and n are fitting parameters.

The last model used here is the bilinear model (8). A bilinear constitutive law (relationship between the true stress and the true strain) is defined by the elastic modulus E, the yield stress and the work hardening rate β.

The model is expressed by the following equations for the stress σ_I:

$$\sigma_i = E\varepsilon_i \quad \text{if } \sigma_i \geq \sigma_y \tag{9}$$

$$\sigma_i = \sigma_y + \beta(E\varepsilon_i - \sigma_y) \quad \text{if } \sigma_i < \sigma_y \tag{10}$$

with $0 \leq \beta \leq 1$; $\beta = 1$ for ideal elastic materials, $\beta = 0$ for ideal plastic materials.

5 Modeling the titanium dioxide elasto-plastic behavior

Shown in Fig. 3 are the contour plots of von Mises stress at different instances of indenter penetration into the pure titanium dioxide layer. Fig. 3c matches the penetration depth being equal to 50 nm, and Fig. 3e shows the stress state after withdrawal of the indenter from the material. After withdrawal of the indenter the material did not return to the initial shape of the specimen, but the indenter leaves an imprint on the surface of the specimen, indicating that plastic deformation occurs during testing, as confirmed by experimental observations. The indentation depth was limited to 50 nm which represents 10 % of the size of the model. After 10 % indentation depth the substrate will influence the results.

For the definition of the stress-strain curve of titanium dioxide three different models have been applied, Hollomon, Ramberg-Osgood and bilinear material model.

The stress-strain curves to be taken as an input for the FE-simulations of the nanoindentation tests which match the Hollomon constitutive behavior are represented in Fig. 4. The corresponding load-displacement curves, obtained as output from the FE-nanoindentaton simulations with these stress-strain curves as input and an experimentally defined load-displacement curve are depicted in Fig. 4b.

The input stress-strain curves for the Ramberg-Osgood constitutive law are depicted in Fig. 5a and the corresponding force-penetration curves obtained from the FE-simulations of nanoindentation tests are depicted in Fig. 5b.

As the Young's modulus for TiO_2 is known from experiments, the parameters σ_y, α and n are determined using inverse analysis.

The bilinear constitutive law has been applied to the TiO_2 material while its elastic modulus has been determined experimentally.

Fig. 6b shows the indentation force-penetration curves for pure titanium dioxide for different input stress-strain curves with a maximum indentation depth of 50 nm. Fig. 6a represents the input stress-strain curves for titanium dioxide with different work-hardening coefficient. The comparison of the resulting force-penetration

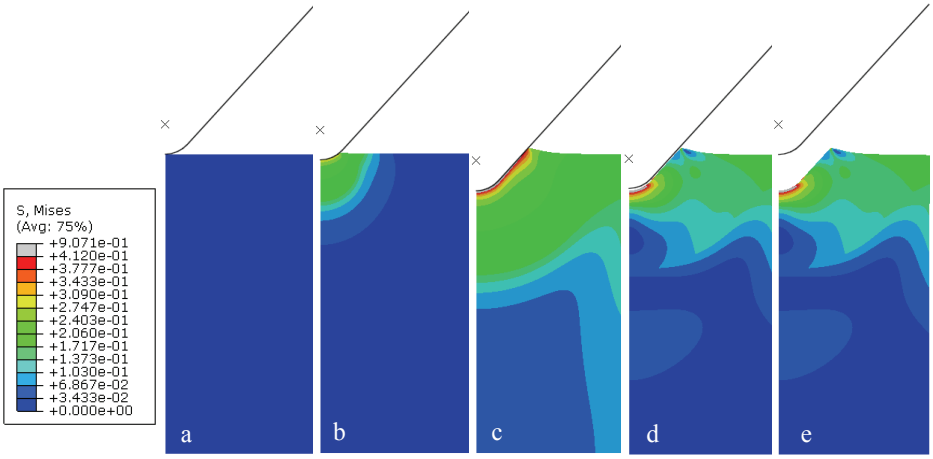

Figure 3: Contour plots of von Mises stress obtained as a result of the FE-simulations of the nanoindentation test of a TiO_2 single layer at different instants of the penetration depth: a) beginning of the nanoindentation test (0 nm); b) 25 nm; c) 50 nm;d) 25 nm; e) 0 nm.

curves for pure titanium dioxide obtained from the FE simulations with the one, obtained in the experiment is represented in Fig. 6b.

It can be seen from Fig. 6b that the dash-dot-dot-curve(σ_y = 0.9 GPa and h = 0) and the dash-dot-dash-curve (σ_y = 0.2 GPa and h = 5.44) represent the best fit for the experimentally obtained force-penetration curve (dash-dot-dot-curve and dash-dot-dash-curve) in Fig. 6a.

The best fit of the force-penetration curves, obtained via inverse modeling following different constitutive laws to the experimentally obtained one are represented in Fig. 7.

It can be observed that among the most fitting curves the best fit to the experimentally defined force-penetration curve is the elastic-perfectly plastic constitutive law with a Young's modulus being equal to 27 GPa and a yield stress of σ_y = 0.9 GPa (dash-dot-dot-curve).

6 Modeling the PE elastoplastic behavior

Having defined the stress-strain curve for the TiO_2 phase, the same procedure has been used to define the stress-strain behavior of the PE-phase. The experiments

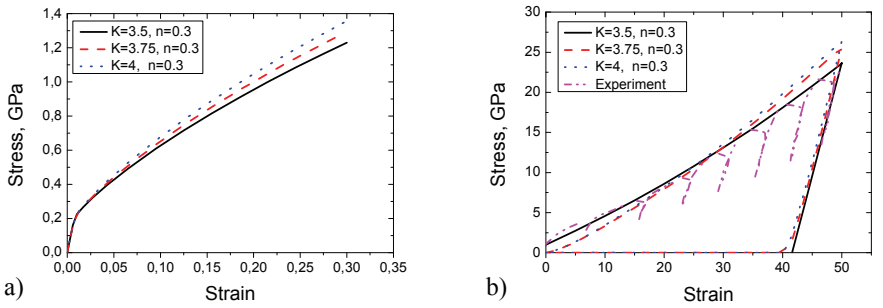

Figure 4: a) Variation of input stress-strain curves for $TiO_2$with fixed parameters: Young's modulus $E = 27$ GPa and Yield stress $\sigma_y = 0.2$ GPa and a variation of Hollomon's constitutive law coefficients: $K = 3.5; 3.75; 4$, ($n = 0.3$ GPa); b) Comparison of the force-penetration curves, obtained from experiments on nanoindentation (dash-dot-dot-curve) and from the FE-simulations for different parameters of Hollomon's constitutive law. The best fit to the experimental force-penetration curve gives the curve obtained from the FE-simulation of the nanoindentation test with a constitutive behavior following Hollomons constitutive law with the parameters $K = 4$ and $n = 0.3$.

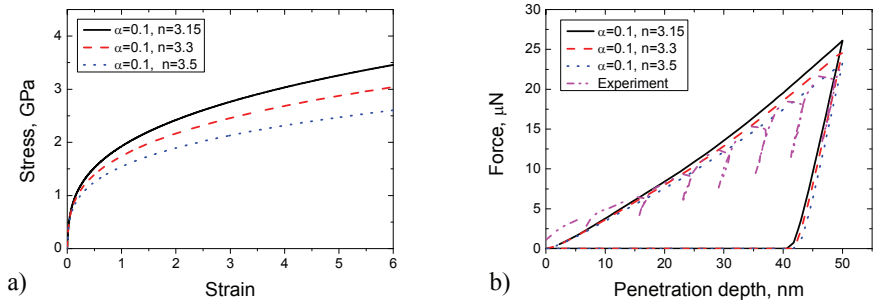

Figure 5: a) Variation of the input stress-strain curves for TiO_2 with fixed parameters: Young's modulus $E = 27$ GPa and yield stress $\sigma_y = 0.2$ GPa and a variation of the Ramberg-Osgood constitutive law coefficients: $n = 3.15; 3.3; 3.5$, ($\alpha = 0.1$ GPa); b) The comparison of the force-penetration curves, obtained from the experiments on nanoindentation (dash-dot-dot-curve) and from the FE-simulations for different parameters of the Ramberg-Osgood constitutive law.

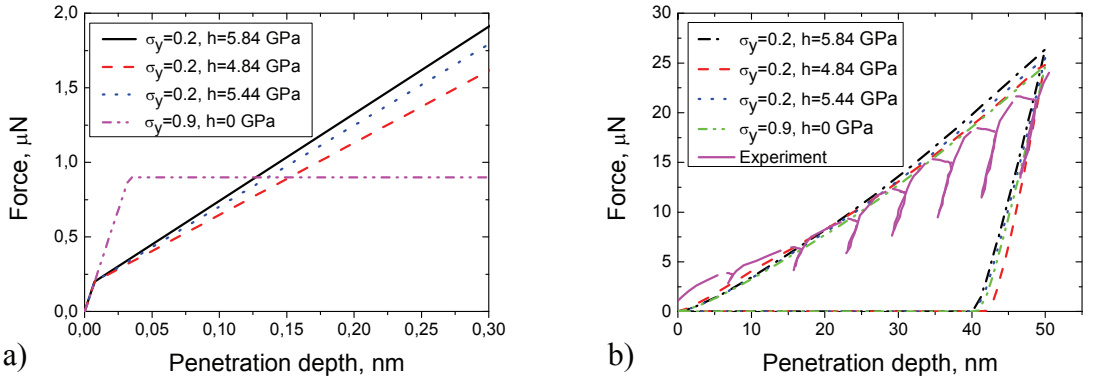

Figure 6: a) Variation of input stress-strain curves for TiO_2 with fixed parameters: Young's modulus E = 27 GPa and yield stress σ_y = 0.2 GPa and variation of work-hardening coefficient: h = 5.84, 4.84 and 5.44 GPa (according to eq. 7); b) The comparison of force-penetration curves, obtained from nanoindentation experiments (continuous line) and from FE-simulations with a variation of parameters like in Fig. 6a.

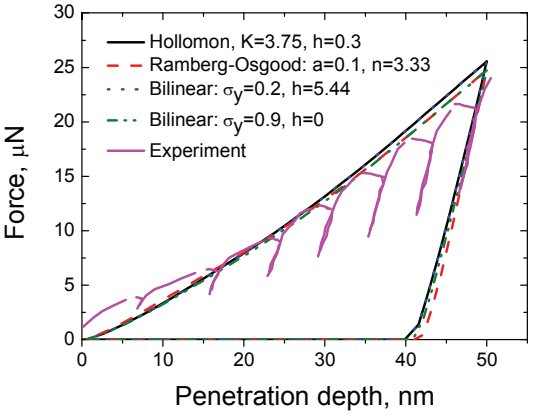

Figure 7: Best fitted force-penetration curves, obtained from the FE-simulations of nanoindentation tests obtained from the stress-strain curves according to different constitutive laws.

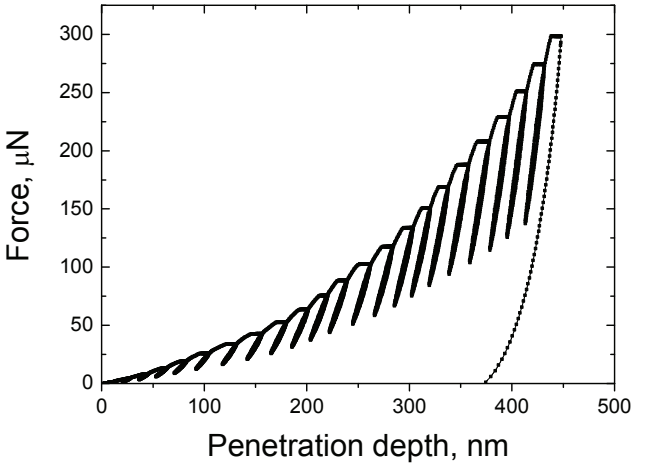

Figure 8: The experimentally obtained force-penetration depth curve from nanoindentation.

on nanoindentation of single layer of polyelectrolyte have been performed. Cube corner indenter penetrates the PE-layer with 500 nm thickness till the penetration depth of 477 nm. The experimentally obtained Force-penetration curve is represented in Fig. 8.

In order to exclude the influence of the silicone substrate, the force-displacement curve obtained in the experiment should be compared, at a penetration depth not exceeding 10-20 % of the film thickness (around 50-70 nm). Inverse modeling of the stress-strain behavior of PE with the Hollomon constitutive law (Fig. 9a) gives the load-displacement curves represented in Fig. 9b.

One can see in Fig. 9 that the best fit of the Force-Penetration curve obtained from FEM-simulations of the nanoindentation test among all input stress-strain curves following Hollomon's constitutive behavior gives the curve with the parameters: $K = 1$, $n = 0.7$.

For the simulations of nanoindentation of PE-phase, the input stress-strain curve of the polyelectrolyte is also approximated with the Ramberg-Osgood equation [8]. A number of iterations have been performed with adjustments of the parameters, and n respectively (Fig. 10a). The corresponding force-penetration curves are depicted in Fig. 10b. The best fit to the experimental curve is achieved with the Ramberg-Osgood constitutive law with the following parameters: $\alpha = 0.1$, $n = 3.2$.

The nanoindentation simulations of the PE film have been also performed with the bilinear constitutive law. The Young's modulus has been taken from the ex-

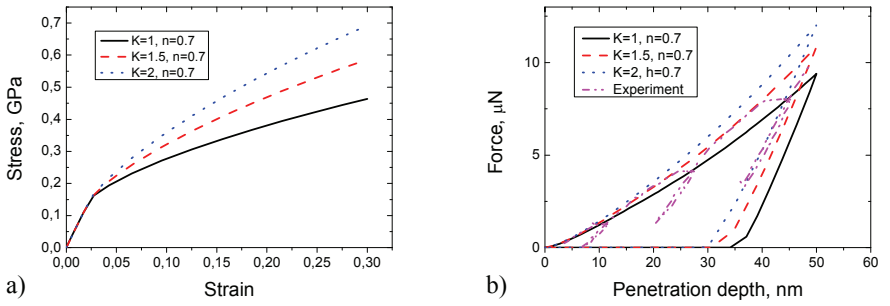

Figure 9: a) Variation of the input stress-strain curves for PE following the Ludwig-Hollomon constitutive law with a variation of the following parameters: K = 1,n = 0.7; K = 1.5, n = 0.7; K = 2, n = 0.7; b) Comparison of the force-penetration curves, obtained from experiments on nanoindentation (dash-dot-dot-curve) and from FE-simulations with Hollomon's constitutive law with different parameters.

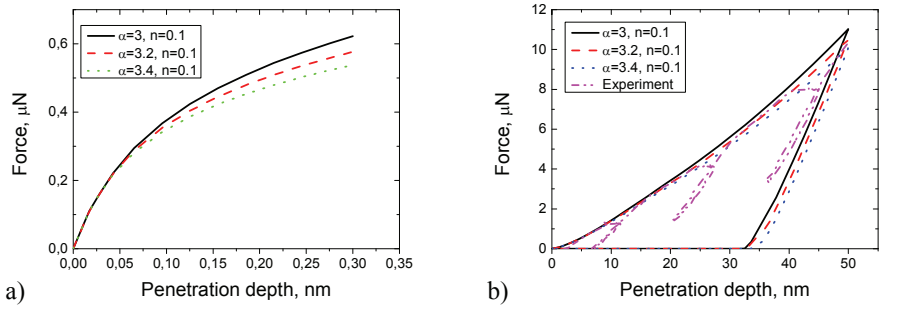

Figure 10: a) Stress-strain curves, obtained according to the Ramberg-Osgood equation with different parameters; b) Force-penetration curves, obtained as a result of the FE-simulations of nanoindentation test with the input stress-strain curves from Fig. 10a as input.

periment and the yield stress and work-hardening have been varied till the force-penetration curve obtained from the FE-simulations achieves the closest fit to the experimentally obtained one. As can be seen from Fig. 11a, two stress-strain bilinear constitutive stress-strain curves σ_y = 0.1 GPa, h = 3.98 GPa and σ_y = 0.2 GPa, h = 2.91 GPa give the same force-penetration curve in Fig. 11b. The elastic perfectly plastic stress-strain curve gives the best fit to the experimentally obtained one among all other curves of the bilinear constitutive behavior.

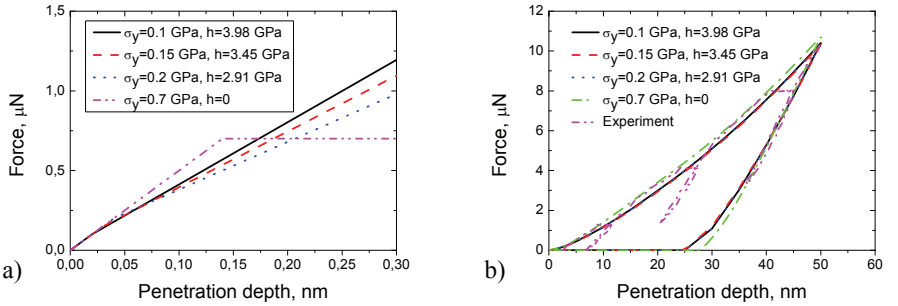

Figure 11: a) Variation of the input stress-strain curves for PE with Young's modulus E = 5 GPa and variation of the yield stress and the work-hardening coefficient: σ_y = 0.1 GPa, h = 3.98 GPa ;σ_y = 0.15 GPa, h = 3.45 GP; σ_y = 0.2 GPa, h = 2.91 GPa; σ_y = 0.7 GPa, h = 0 GPa; b) Comparison of the force-penetration curves, obtained from the FE-simulations with the stress-strain curves of Fig. 11a as input, with the one obtained from experiments on nanoindentation (dash-dot-dot-curve).

The best fit of the force-penetration curves for PE, obtained via inverse modeling following different constitutive laws to the experimentally obtained one, are represented in Fig. 12.

The Young's modulus being equal to 5 GPa has been taken from the experiment and following the equation 8, the work–hardening parameter has been adjusted till the experimental curve fits the computed one (Fig. 6b). The stress-strain curve with σ_y = 0.7 GPa and with perfect plasticity has been determined as the constitutive law for the polyelectrolyte film.

7 Conclusions

In the present work, finite element modelling was successfully utilized to simulate the nanoindentation of the films obtained by chemical bath deposition technique

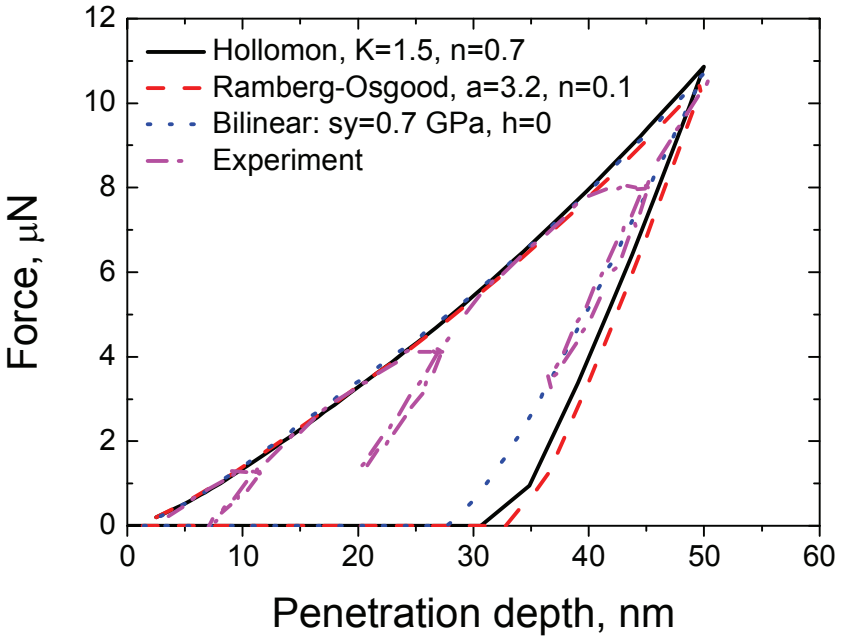

Figure 12: Best fit force-penetration curves, obtained from FE-simulations of nanoindentation tests obtained from stress-strain curves according to different constitutive laws. Young's modulus was taken from the experiment (5 GPa).

(TiO_2) and layer by layer technique (PE) to obtain the mechanical properties (elastic and plastic properties) of inorganic (TiO_2) and organic (PE) thin films.

The output force-penetration curves, obtained from the FE-simulations of nanoindentation tests of thin TiO_2 and PE films based on inverse modelling with taking into account the input stress-strain curves following different constitutive laws have been compared with force-penetration curves, obtained from the experiment.

For the TiO_2 film, the force-penetration curves, obtained from the FE–simulations of nanoindentation tests is obtained being identical to the experimental one either with lower yield σ_y = 0.2 GPa and work-hardening (h = 5.44), or with perfect plasticity and higher yield stress (σ_y = 0.9 GPa). For the polyelectrolyte film the force-penetration curve, obtained from the FE–simulations of nanoindentation tests, is obtained being identical to the experimental one with perfect plasticity and stress (σ_y = 0.9 GPa).

The work-hardening behaviour and higher yield stress of ceramics (TiO_2) and organic (PE) are not typical for materials produced by chemical bath deposition technique (TiO_2) and layer-by-layer deposition technique (PE). For amorphous or non-metallic materials, the work-hardening is assumed to be very low (9). Both effects could be explained by the manifestation of the influence of the more rigid substrate. In the present work we did not take into account the influence of the substrate, assuming that at the shallow penetration of 10 % there is no influence of the substrate. The ambiguity of bilinear stress-stain constitutive law with work-hardening and without it (with perfect plasticity) will be the topic of our further investigations.

Acknowledgement: The authors acknowledge funding by the German Research Foundation (Deutsche Forschungs gemeinschaft, DFG), project number Schm 746/88-1.

References

1. Barthelat F (2007) Biomimetics for next generation materials. *Philosophical transactions Series A, Mathematical, physical, and engineering sciences* 365:2907–19.

2. Burghard Z et al. (2007) Nanomechanical Properties of Bioinspired Organic–Inorganic Composite Films. *Advanced Materials* 19:970–974.

3. Burghard Z et al. (2009) Toughening through nature-adapted nanoscale design. *Nano letters* 9:4103–8.

4. Oliver W, Pharr G (1992) An improved technique for determining hardness

and elastic modulus using load and displacement sensing indentation experiments. *Journal of Materials Research* 7 (6):1564–1583.

5. Kopernik M, Szeliga D (2007) Modelling of nanomaterials-sensitivity analysis with respect to the material parameters. *Computer Methods in Materials Science* 7:255–261.

6. Hollomon J (1945) Tensile deformation. *Transactions of the American Institute of Mining, Metallurgical and Petroleum Engineers* 162:268–290.

7. Ramberg W, Osgood W (1943) Description of stress-strain curves by three parameters. *National Advisory Committee for Aeronautics, Washington, DC, Technical Note No 902* 07.

8. Kopernik M, Pietrzyk M (2007) 2D numerical simulation of elasto-plastic deformation of thin hard coating systems in deep nanoindentation test with sharp indenter. *Archives of Metallurgy and Materials* 52:299–310.

9. Knapp J a., Follstaedt DM, Myers SM, Barbour JC, Friedmann T a. (1999) Finite-element modeling of nanoindentation. *Journal of Applied Physics* 85:1460.